Flexible Transparent Supercapacitor with Core-shell Cu@Ni@NiCoS Nanofibers Network Electrode

Soram Bobby Singh, Thangjam Ibomcha Singh, Dai Jiu Yi, Tolendra Kshetri, Nam Hoon Kim, Joong Hee Lee

PII: S1385-8947(20)31011-1
DOI: https://doi.org/10.1016/j.cej.2020.125019
Reference: CEJ 125019

To appear in: *Chemical Engineering Journal*

Received Date: 13 January 2020
Revised Date: 1 April 2020
Accepted Date: 6 April 2020

Please cite this article as: S. Bobby Singh, T. Ibomcha Singh, D. Jiu Yi, T. Kshetri, N. Hoon Kim, J. Hee Lee, Flexible Transparent Supercapacitor with Core-shell Cu@Ni@NiCoS Nanofibers Network Electrode, *Chemical Engineering Journal* (2020), doi: https://doi.org/10.1016/j.cej.2020.125019

Flexible Transparent Supercapacitor with Core-shell Cu@Ni@NiCoS Nanofibers Network Electrode

Soram Bobby Singh[a], Thangjam Ibomcha Singh[a],Dai Jiu Yi[a], Tolendra Kshetri[a], Nam Hoon Kim[a], Joong Hee Lee[a, b,*]

[a]Advanced Materials Institute of BIN Convergence Technology (BK21 plus Global) and Department of BIN Convergence Technology, Chonbuk National University, Jeonju, Jeonbuk, 54896, Republic of Korea

[b]Carbon Composite Research Centre, Department of Polymer-Nano Science and Technology, Chonbuk National University, Jeonju, Jeonbuk 54896, Republic of Korea.

*Corresponding author: e-Mail: jhl@chonbuk.ac.kr (Joong Hee Lee)

Abstract

Transparent flexible supercapacitors are crucial for the progress of high-tech modern transparent wearable electronic gadgets. Thus, fabricating high opto-electrochemical performance electrodes is crucial for the development of high energy density transparent flexible supercapacitors. Herein, direct growth of battery-type ternary nickel-cobalt sulfide (NiCoS) nanosheets on Cu@Ni NFs network transparent electrode forming a seamless Cu@Ni@NiCoS NFs core-shell electrode structured is reported to boost the energy density of transparent supercapacitors. The core Cu@Ni nanofibers network electrode exhibited both excellent electro-optical performance (sheet resistance~12.19 Ω/sq at ~89 % transmittance) and high mechanical flexibility. NiCoS thin

nanosheets shell offer high porosity, abundant active sites, and large electrode-electrolyte contact area, thus facilitating the fast diffusion of electrolytes into active materials. The Cu@Ni@NiCoS NFs core-shell electrode demonstrated remarkable high opto-electrochemical performance (transparency of ~76.83%, an areal capacity of 6.94 μA h/cm^2, and high rate capability) and excellent mechanical properties. Finally, a transparent flexible symmetric supercapacitor device (SSC device) assembled by employing Cu@Ni@NiCoS NFs as both electrodes demonstrates an outstanding energy density of 0.48 μW h/cm^2 at a power density of 11.15 μW/cm^2 with device transparency of ~65 %.

Keywords: Core-shell, Energy density, Flexible, Nanofibers, Transparent, Supercapacitor

1. Introduction

Currently, with the fast-growing progress of wearable and transparent electronic gadgets, developing of high energy density transparent and flexible energy storage devices is urgently needed [1–4]. Among reported transparent energy storage devices, transparent and flexible supercapacitors are of great interest owing to their high transparency, flexibility, excellent areal capacitance, long-term GCD (Galvanostatic charge-discharge) stability, high power density, and low cost [5–7]. However, to develop a high energy density transparent flexible supercapacitor, the electrode materials should not only possess high electro-optical performance but should also have plenteous redox-active sites i.e. high electrochemical performance [6,8–11]. The high electro-optical electrode material guarantees fast electron transport capability of the electrode at high transparency while having plenteous redox-active sites will enhance the electrochemical performance i.e. achieving a high energy density of the device. But most of the high energy density electrode materials are generally opaque and hence, it is still a great challenge to obtain a high

energy density transparent flexible supercapacitor device [12]. To date, several flexible transparent supercapacitor devices have been demonstrated using carbon-based active electrode materials (such as grapheme [13,14] and carbon nanotubes [15–17]), conducting polymer films [18–22] and metal network-based electrodes [23–33].Compared to carbon-based and conducting polymer electrode materials where the electrochemical performance is mainly defined by the electric double-layer capacitance (EDLC), metal network electrodes-based supercapacitor electrodes have gained intense attention owing to their ability to deposit diversified active materials, both EDLC and pseudo-capacitive materials, demonstrating high areal capacitance at high transparency [6,7,12,30-33]. Additionally, the growth of abundant redox-active site materials on the metal network can lead to more attractive structure-related features towards the fabrication of high energy density transparent flexible supercapacitors [6,7,32,33]. For example, MnO_2@Au nanofiber network, AgNWs@NiCo/$NiCo(OH)_2$ core-shell nanostructures, $Co(OH)_2$@AgNws network electrodes demonstrated excellent electrochemical performances at high transparency [7,32,33]. Among them, the MnO_2@Au nanofiber network electrode showed promising optical and electrochemical results (areal capacitance ~8.26 mF/cm^2 at ~86% transmittance) [7]. Thus, with proper selection of diversified active materials in cooperation with a high-performance electro-optical metal network electrode, one can achieve greater electrochemical performance at high transparency. Among the reported various high pseudo-capacitive materials, ternary transition metal sulfides have been extensively studied and display outstanding electrochemical performance owing to their higher conductivity, abundant redox-active metal species, and synergistic effects of each constituents elements [34–40]. For example, a recent study on a ternary metal sulfide material grown on a carbon cloth support has demonstrated a remarkable capacitance ~1418 F/g at 5 A/g [41]. The fabricated asymmetric device also demonstrated a high energy density

and power density of 60 Wh/kg and 1.8 kW/kg, respectively. However, the application of metal sulfides films for flexible transparent supercapacitor electrode is limited due to opaqueness (black in color). Moreover, there are no reports on the application of metal sulfides yet, especially Ni-Co-S materials for transparent flexible supercapacitor to the best of our knowledge. Thus, nickel-cobalt sulfides might be the best choice as active electrode materials for high performance transparent flexible supercapacitor fabrication because of their excellent electrochemical performance and ease of direct growth by a simple electrodeposition technique [41–45].

Currently, the most commonly reported metal network supercapacitor electrodes are produced with the gold metal network, [7,12,28,30] as gold is electrochemically very stable. However, gold is very expensive and thus limits the cost-effective production of flexible transparent supercapacitors. In addition, the reported electrode fabrication techniques are either complicated or harmful to the environment [12,23,27]. Hence, the development of a simple and low-cost high-performance metal network-based electrode in replacement of expensive gold electrode is urgently needed. Recently, the copper network-basedtransparent electrode has drawn a lot of attraction owing to the low cost, high abundance, and silver-like electrical conductivity of the copper metal. For example, electrospun based copper nanofiber/nanotroughs network electrode has been reported to have the best electro-optical performance (~2 Ω/sq at 90~ % T) [46]. However, they suffer from several drawbacks such as a high tendency to undergo surface oxidation even at room temperature when they are exposed to humid environments and poor chemical stability which makes them unsuitable for use as transparent current collectors in energy storage applications [47–50]. As a result, there has been no report on the utilization of copper network electrode-based transparent flexible supercapacitors. Thus, searching for an effective facile method is still needed

to develop highly conducting, oxidation resistant Cu based network electrode for transparent flexible energy storage applications.

Herein, we reported the successful fabrication of a high performance flexible transparent battery-type supercapacitor electrode based on nickel encapsulated copper nanofibers (Cu@Ni NFs) network electrode and active Ni:Co sulfides with a unique core-shell nanofibers network electrode using scalable electrospinning, metal deposition, and electrodeposition techniques. The distinct Cu@Ni@NiCoS NFs network electrode structure might offer several advantages. First, the deposition of the thin Ni layer over the Cu NFs will improve the electrochemical stability, oxidation resistance, high thermal stability and the greater pH endurance of the transparent electrode. Secondly, selective direct growth of high-performance ternary NiCoS nanosheets shell over Cu@Ni NFs network electrode by electrodeposition technique might not only improve the electron transport efficiency at the interfaces of the current collector and active NiCoS nanosheet but also maintain high transparency of the electrode. Thirdly, the porous structure of the ternary NiCoS nanosheets over Cu@Ni NFs network electrode might provide more active redox sites to enable the quick passage of electrolyte ions which in turn contribute high electrochemical performance. The hierarchically interconnected Cu@Ni@NiCoS NFs network electrode displayed an exceptional high areal capacity of 6.94 μA h/cm^2 and ~76.83 % transmittance. The electrode also showed long term charge-discharge stability, high rate capability, and excellent mechanical flexibility. Lastly, a transparent flexible symmetric solid-state supercapacitor device (SSC device) was assembled using two similar Cu@Ni@NiCoS NFs network electrodes and the device demonstrated an exceptional electrochemical performance with a high energy density of 0.48 μW h/cm^2 at a power density of 10 μW/cm^2.

2. Experimental Section

2.1. Fabrication of Cu@Ni NFs network electrode

Free-standing nickel encapsulated copper-coated PVA nanofibers (Cu@Ni NFs) network was fabricated using E-beam deposition and electrospinning techniques employed in our previous report [51]. The same conditions of the electrospinning process for the PVA nanofiber web used in our earlier reported work were used in the present study [51]. Here, a 70 nm thick copper (Cu) was initially deposited over the free-standing PVA nanofiber template followed by the deposition of another 30 nm thin Ni films using an electron-beam evaporation system (BSVAC E-Beam Evaporator) at a deposition rate of 0.3 Å/s and a base pressure of ~(1-2)x10^{-6} Torr, resulting in a Cu@Ni NFs network electrode. To compare oxidation resistance performance, a bare Cu NFs network electrode with a thickness of 100 nm was also fabricated using the same process as mentioned above.

2.2. Fabrication of core-shell Cu@Ni@Ni:Co-S NFs network electrode

Core-shell Cu@Ni@Ni:Co-S NFs network electrode was fabricated by direct growing of Ni:Co-S nanosheets on Cu@Ni NFs network electrode using the potentiostatic deposition technique in a three-electrode electrochemical setup (CH660E electrochemical workstation) with Cu@Ni NFs network electrode (2 cm x 4 cm) as working electrode while Platinum (Pt) plate was used as the counter electrode and Ag/AgCl as the reference electrodes, respectively. The electrolyte solution was prepared by dissolving 0.75 M thiourea ($CS(NH_2)_2$) and 5 mM of $NiCl_2.6H_2O$:$CoCl_2.H_2O$ (in different ratios; 0:1, 0.1:0.9, 0.2:0.8, 0.5:0.5, 0.8:0.2, 0.9:0.1, and 1:0, respectively) in 50 ml of DI water under continuous magnetic stirring to obtain different compositions of Ni:Co-S. Electrodeposition was carried out in each electrolyte solution at an operating voltage of -0.9 V (vs.

Ag/AgCl) for a fixed duration of 20 min. Hereafter, resulting samples are presented as CoS, NCS-1, NCS-2, NCS-3, NCS-4, NCS-5, and NiS, respectively. With DI water and ethanol, the electrodeposited samples were washed thoroughly several times to remove any residual electrolyte and dried at 60^{o}C in a vacuum oven for 12 hr. After that, the best composition of Ni:Co-S was further studied with different electrodeposition time to optimize it for high opto-electrochemical performance.

2.3. Fabrication of Transparent flexible Symmetric Solid-State Supercapacitor (SSC) Device

Transparent flexible symmetric solid-state supercapacitor (SSC) device was fabricated using two similar Cu@Ni@NiCoS NFs network electrode as electrodes and PVA-KOH gel as an electrolyte. To prepare PVA-KOH gel electrolyte, 2.0 g of PVA was initially dissolved in 10 ml of DI water by heating for 2 h at the temperature of 85^{o}Cfollowed by a dropwise addition of 10 ml of 1.7 M KOH aqueous solution. The PVA-KOH solution mixture was further maintained at 85°C under continuous stirring for another 3 h to obtain a transparent solution. Two identical Cu@Ni@NiCoS NFs network electrodes were then dipped into the PVA-KOH gel electrolyte for 30 min and dried in free air for 15 min (area of the coated gel-electrolyte = 2x1 cm^2). These dried samples were again dipped into the gel electrolyte and then gently assembled by pressing together to the finally obtained transparent flexible SSC device. The device was then kept at room temperature for 24 hr before performing electrochemical tests.

2.4. Characterization

Surface morphologies of the electrode samples were studied using FE-SEM, Carl Zeiss, SUPRA 40 VP, Germany, at the Centre for University-wide Research Facilities (CURF), Jeonbuk National

University, Korea. The internal structure, elemental composition, and spatial distribution of constituent elements were investigated using a high-resolution transmission electron microscope (HRTEM), a scanning transmission electron microscope (STEM) (JEM-2200 FS; JEOL Ltd., Japan, 200 kV), and energy-dispersive X-ray spectroscopy (EDX). The crystallinity and phase of the samples were identified using X-ray diffraction (Rigaku Corporation, Japan, CuKα radiation, wavelength =0.154 nm in the 2θ range of 10-70^{o}at the slow scan rate of 2^{o}/min.The chemical compositions and elemental states of Cu@Ni@NiCoS NFs network electrode were studied using an X-ray photoelectron spectroscopy (XPS) (Theta Probe AR-XPS System, Thermo Fisher Scientific, UK) at the KBSI Centre, JBNU campus. Transparencies of electrode samples and devices were analyzed using Jasco-ARSN-733 UV-Vis-NIR spectroscopy. Using a four-point-probe surface resistivity meter (MSTEC) coupled with a Keithley-2182A nano voltmeter having a Keithley-6221 DC/AC current source the sheet resistance of the electrode samples were measured. Mechanical flexible properties were tested with a Radius Bending Tester-JIRBT-610 coupled with a Keithley-6221 DC/AC current source.A CH660E electrochemical workstation (CH Instruments, Inc., USA) was used to characterize the electrochemical performance of the single electrode (Cu@Ni@NiCoS NFs) and the fabricated SSC device in the mode of three and two-electrode configurations, respectively.

3. Results and discussions

The fabrication process of Cu@Ni@NiCoS NFs network transparent flexible supercapacitor electrode and the SSC device is shown in the schematic diagram, Fig. 1. First, by using an

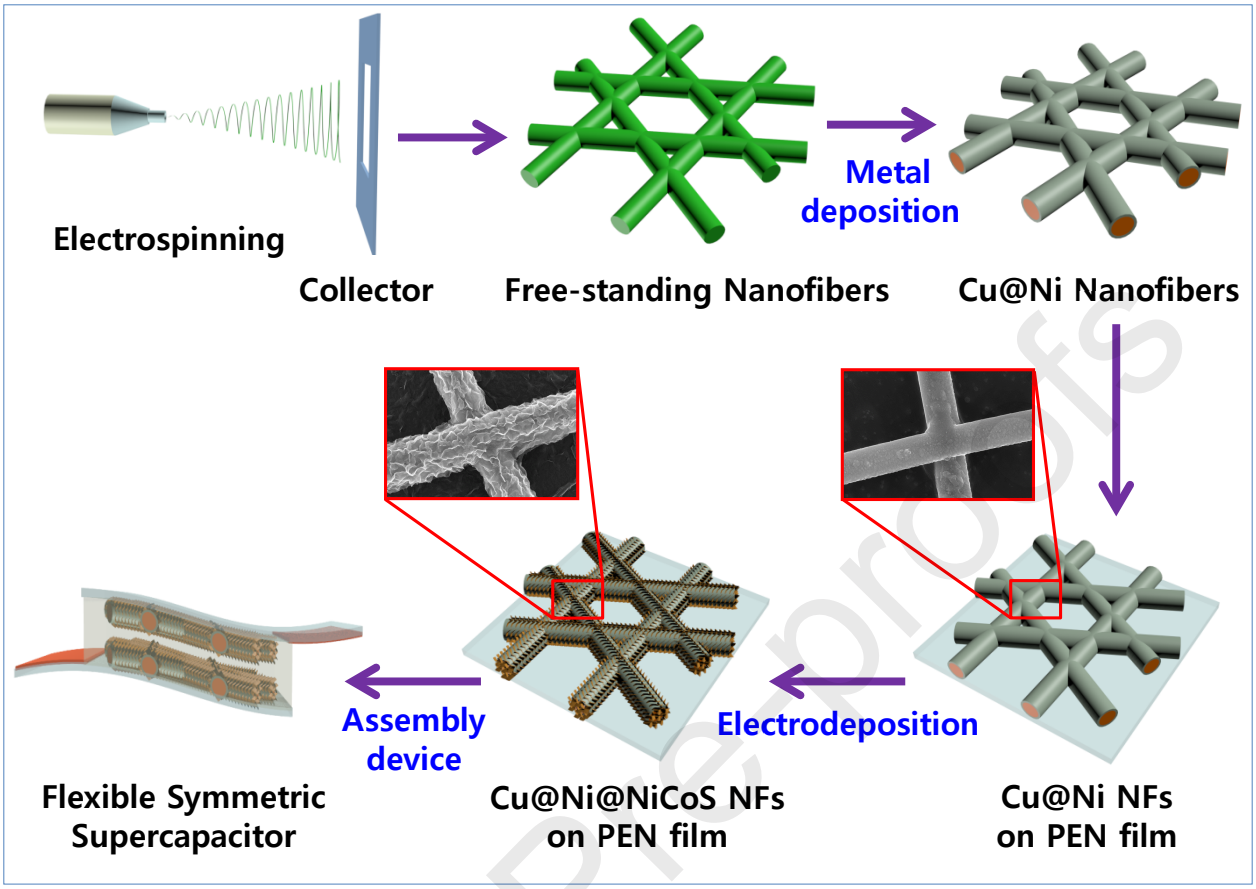

Fig. 1. Schematic illustration for the fabrication of intertwined Cu@Ni@NiCoS NFs network transparent flexible supercapacitor electrodes and transparent flexible SSC device.

electrospinning process, a free-standing PVA nanofiber network was collected on a metallic frame followed by thermal deposition of copper on both sides of the nanofiber to obtain a free-standing Cu NFs network similar to our previously reported work [51]. Second, the Cu NFs network was encapsulated by coating a thin layer of Ni film to obtain an oxidation-resistant Cu@Ni NFs network electrode. The Cu@Ni NFs network was subsequently transferred on a polyethylene naphthalate (PEN) substrate similar to our previous work [51]. Thirdly, interconnected NiCoS nanosheet was then directly grown over the Cu@Ni NFs network electrode using the

electrodeposition process, yielding to a unique Cu@Ni@NiCoS NFs core-shell flexible NFs network electrode structure.

As mentioned above, the replacement of expensive gold metal with other inexpensive metal with high chemical stability is of urgent need. So, we fabricated nickel encapsulated copper nanofiber (Cu@Ni NFs) network electrode as a replacement of gold metal, using the same fabrication technique as reported in our previous work [51]. Here, we are using nickel as a protective layer of Cu NFs, as nickel is chemically very stable compare to silver or copper, less expensive compared to gold and also shows almost similar conductivity. It is very important to acknowledge that for the application of supercapacitor, the chemical stability of the transparent current collector (transparent electrode) against a strong acidic and basic environment is of great concern. In specific, the corrosion of a transparent supercapacitor electrode by harsh chemical medium can damage the interface, thus reducing the performance of the supercapacitor electrode. This phenomenon is associated with Cu NFs as compared to Au NFs because of the stronger chemical activity of Cu film. To understand the corrosion resistance/chemical stability, we studied the chemical/thermal stability of the Cu@Ni NFs network in comparison with the bare Cu NFs network. In acidic medium, the Cu@Ni NFs exhibited significant resistance against corrosion while the bare Cu NFs showed poor corrosion resistance (Fig. S1a). To confirm any surface degradation of the pure Cu NFs and Cu@Ni NFs network during the acid test, we characterized surface morphologies of these electrodes by FE-SEM (Fig. S1b,c) after the acid test. It was observed that the surface of the bare Cu NFs degraded after 1 min, indicating weak chemical stability toward an acid medium (Fig. S1b). However, no such surface degradation was observed in Cu@Ni NFs network (Fig. S1c), suggests its strong chemical stability in an acid medium. Effects of humidity ($60 \pm 10\%$) and temperature ($80^{o}C$) on sheet resistance of the bare Cu NFs and

Cu@Ni NFs network electrodes with respect to time were also investigated. The results are shown in (Fig. S1 d-f). The detailed study is highlighted in the Supplementary Information.From the above experimental results, it is confirmed that Cu@Ni NFs network electrode demonstrated a significant improvement in both chemical stability and oxidation resistance under a high humid environment compared to bare Cu NFs network electrode which showed an extremely high oxidation rate. Hence, Cu@Ni NFs network electrode might be the best candidate as a replacement of gold metal for the fabrication of high-performance flexible transparent energy storage devices. The electro-optical properties of the Cu@Ni NFs network electrode will be discussed in the later section.

Using Cu@Ni NFs network as a transparent flexible current collector various compositions of ternary nickel-cobalt sulfide (Ni:Co-S) nanosheets were then electrodeposited over the Cu@Ni NFs network electrode to study the synergistic effects of Ni and Co in the ternary Ni:Co-S nanosheet structure and to optimize the best Ni:Co composition. The preparation of the electrolyte solutions for Ni/Co ratio optimization is mentioned clearly in the Experimental section. Notably, the electrodeposition of ternary metal sulfides over the Cu@Ni NFs provides a simple method for large-scale fabrication of transparent flexible energy storage devices. Fig. S2shows FE-SEM photographs of NCS-1 to NCS-5 representing different compositions of electrodeposited Cu@Ni@Ni:Co-S NFs network electrodes. As shown in Fig. S2,the morphology of deposited Ni:Co-S nanosheets structure changed from thinly growth large nanosheet with larger inter-sheet gaps (Fig. S2a,b) to the growth of interconnected uniform wrinkle nanosheet structures (Fig. S2e) with increasing concentration of Ni:Co ratios. Further increase in Ni concentration beyond Ni = 0.8 led to a decrease in the size of the nanosheet structure with smaller inter-sheet gaps as shown in Fig. S2f,g. Similar variation in the surface morphology of Ni:Co-S nanosheets with different

Ni:Co ratios have also been observed in previous reports[41–45]. Among all samples, NCS-4 with Ni:Co=0.8:0.2 showed the most uniform and striking features and it is expected to show better electrochemical performance. The successful growth of Ni:Co-S nanosheet over the Cu@Ni NFs can be confirmed from different surface morphologies of the bare Cu@Ni NFs and Cu@Ni@Ni:Co-S NFs (Fig. S3). Different compositions with different surface morphologies of the Ni:Co-S nanosheets compared to the Cu@Ni NFs network electrode are expected to lead todifferent electrochemical performances and will be discussed in the following section.

Electrochemical performances of various compositions of Cu@Ni@Ni:Co-S NFs network electrode (represented by CoS, NCS1 to NCS5 and NiS) were first studied to investigate the best composition of Ni/Co ratio in the ternary Ni:Co-S transparent supercapacitor electrode. Fig. S4a shows the comparative cyclic voltammograms (CV) curves of various compositions of Cu@Ni@Ni:Co-S NFs network electrodes at a scan rate of 10 mV/s. Notably, it was observed that all electrodes showed a pair of redox peaks, indicating that the capacity of these ternary metal sulfide electrodes mainly arose from the Faradaic redox reaction caused by the reversible valence between Ni^{2+}/Ni^{3+} and Co^{2+}/Co^{3+}[52,53]. With an increase of Ni concentration, anodic peaks of the samples were found to be shifted to a higher potential. This shift in higher potential might be due to the higher redox reaction potential of Ni species than its counterpart Co species, similar to previous reports[40,54,55]. In CV curves, NCS-4 (composition Ni:Co = 0.8:0.2) electrode demonstrated higher electrochemical performance, showing a superior redox peak with a large CV area as compared to other samples. Fig. S4b shows comparative Galvanostatic charge-discharge (GCD) characteristics of samples with different compositions at 0.066 mA/cm^2 current density. All electrode samples showed symmetric GCD behaviors along with a negligible voltage drop, demonstrating high ionic conductivity and good electrical properties of ternary sulfides.

Remarkably, the NCS-4 electrode exhibits the longest charging and discharging time compare to the other samples, suggesting best electrochemical performances which further confirm that the best Ni/Co ratio in ternary nickel-cobalt sulfide electrode is 0.8:0.2 i.e the Ni(0.8):Co(0.2). Also, from the FE-SEM photograph (Fig. S2) the composition Ni(0.8):Co(0.2) shows a better and uniform growth of large NiCoS nanosheets over the Cu@Ni NFs network electrode.Areal capacities (C/A) of ternary Cu@Ni@Ni:Co-S NFs network electrodes with different compositions were calculated from both the CV curve and GCD curves using (Eq. S1). Fig. S4c, d show the calculated C/A of the ternary sulfide electrode as a function of Ni:Co ratio, determined from the CV curve. The areal capacities of the ternary Cu@Ni@Ni:Co-S NFs network electrode increased significantly with an increase in the Ni:Co ratio up to a maximum of 0.8:0.2, and then decreased with higher Ni concentration. The sample NCS-4exhibited a high areal capacity of 3.74 μA h/cm^2 at the scan rate of 10 mV/s, much higher than that of 0.83 μA h/cm^2 for pure CoS, 1.12 μA h/cm^2 for NCS-1, 1.29 μA h/cm^2 for NCS-2, 2.23 μA h/cm^2 for NCS-3, 2.22 μA h/cm^2 for NCS-5, or 1.39 μAh/cm^2 for pure NiS. Also, specific capacities of electrodes determined from GCD curves (Fig. S4d) showed similar trends with sample NCS-4 showedhigh specific capacity of 3.17 μA h/cm^2. The large variation in the electrochemical performance of these ternary sulfide materials might be associated with their different morphologies and compositions as highlighted in previously reported works[40,42,44]. From the above electrochemical performances result, it was found that the NCS-4 sample exhibited higher electrochemical performance than other electrodes and is considered as the best-optimized sample and will be termed as Cu@Ni@NiCoS NFs network electrode hereafter.

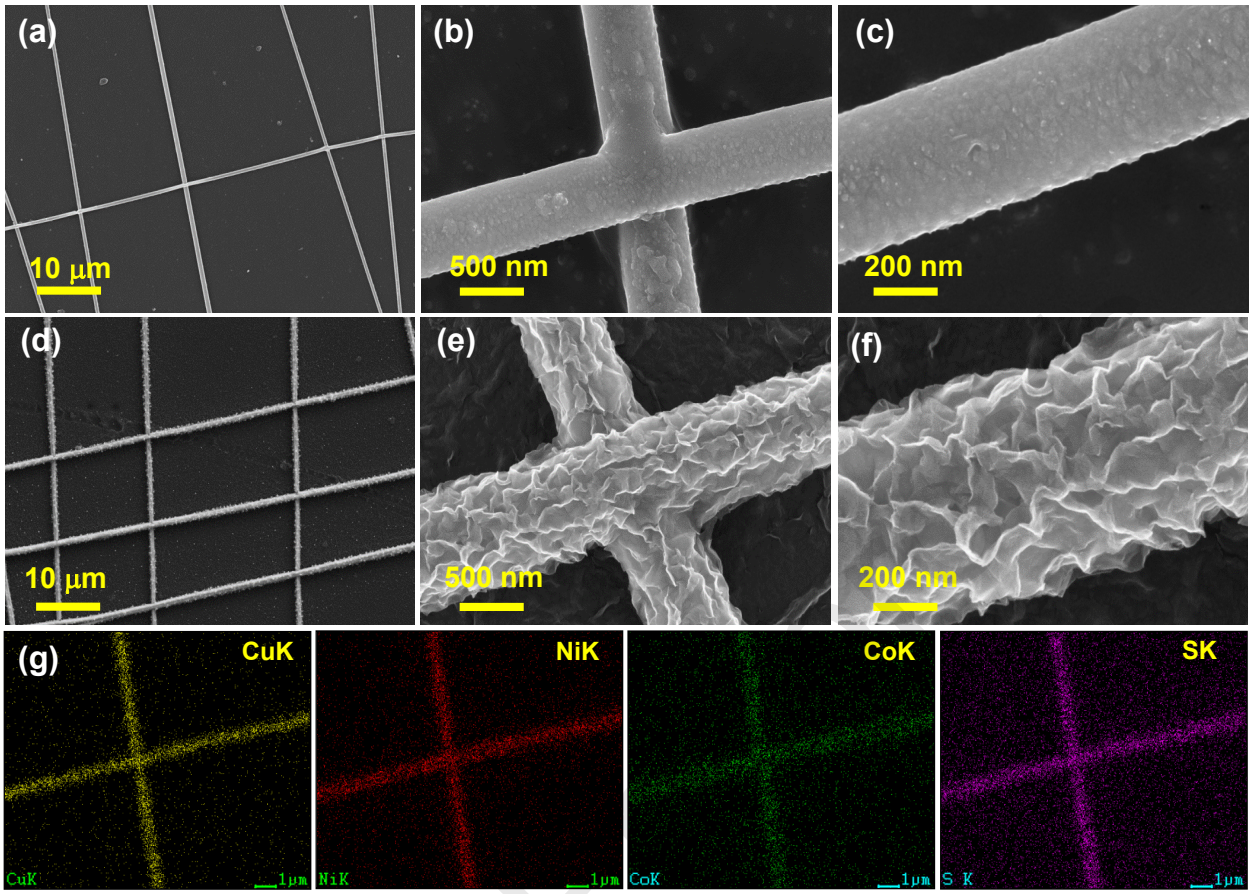

Fig. 2. Surface FE-SEM photographs. (a-c) Cu@Ni NFs network electrode at different magnifications, (d) Electrodeposited intertwined nanosheet Cu@Ni@NiCoSNFs network electrode at low magnification. (e, f) Magnified FE-SEM photograph of Cu@Ni@NiCoS NFs. (g) EDS mapping of Cu@Ni@NiCoS NFs network electrode showing a uniform growth of NiCoS over the Cu@Ni NFs network.

The surface morphologies of the Cu@Ni NFs and Cu@Ni@NiCoS NFs network on the PEN substrate were characterized using field emission scanning electron microscopy (FE-SEM) and FE-SEM photographs are shown in Fig. 2. A uniform Cu@Ni nanofibers distribution having an average Cu@Ni NF diameter of ~300-400 nm along with a large open area network structure was observed, Fig. 2a. FE-SEM photographs also revealed that these Cu@Ni nanofibers network had

high aspect ratios along with junction free network structure. Such network structures of the Cu@Ni NFs network are anticipated to enhance the electrical conductivity of the electrode at high transmittance [7]. Fig. 2b (magnified FE-SEM photograph of Fig. 2a) confirmed the formation of a fused junction. Fig. 2d shows a low magnification FE-SEM photograph of the Cu@Ni@NiCoS NFs network, where the highly conducting Cu@Ni NFs with large open areas acts as an excellent backbone for the homogeneous growth of these ternary metal sulfide nanosheets. High magnification FE-SEM (Fig. 2e) revealed the uniform deposition of NiCoS nanosheets over the Cu@Ni NFs network. Fig. 2f displayed the formation of a dense array of highly porous interconnected wrinkled nanosheets structures of NiCoS on Cu@Ni NFs network. This highly porous interconnected nanosheet morphology of Cu@Ni@NiCoS NFs is favorable for high energy density supercapacitors owing to the enhanced redox-active surface area (i.e., easy diffusion of electrolyte ions throughout electrode materials). Further, EDS (energy-dispersive X-ray spectroscopy) mapping was measured to investigate elemental distributions of constituent elements in the Cu@Ni@NiCoS NFs network electrode. The EDS mapping image of Cu@Ni@NiCoS NFs network demonstrated uniform elemental distributions of Ni, Co, and S over the Cu@Ni NFs (Fig. 2g). The EDS mapping of the bare Cu@Ni NFs network (Fig. S5) also displayed a uniform deposition of Ni over the Cu NFs network by an e-beam deposition process, confirming the formation of the encapsulated Cu@Ni NFs network.

We also studied the internal nanosheet structure of Cu@Ni@NiCoS NFs network electrode by transmission electron microscopy (TEM). Fig. 3 (a-c) shows TEM images of Cu@Ni@NiCoS NFs at different magnifications, demonstrating the successful growth of ultrathin NiCoS nanosheet arrays over the Cu@Ni NFs core, forming the core-shell structure of Cu@Ni@NiCoS NFs. The HAAD-STEM image of Cu@Ni@NiCoS NFs (Fig. 3d) showed a high contrast

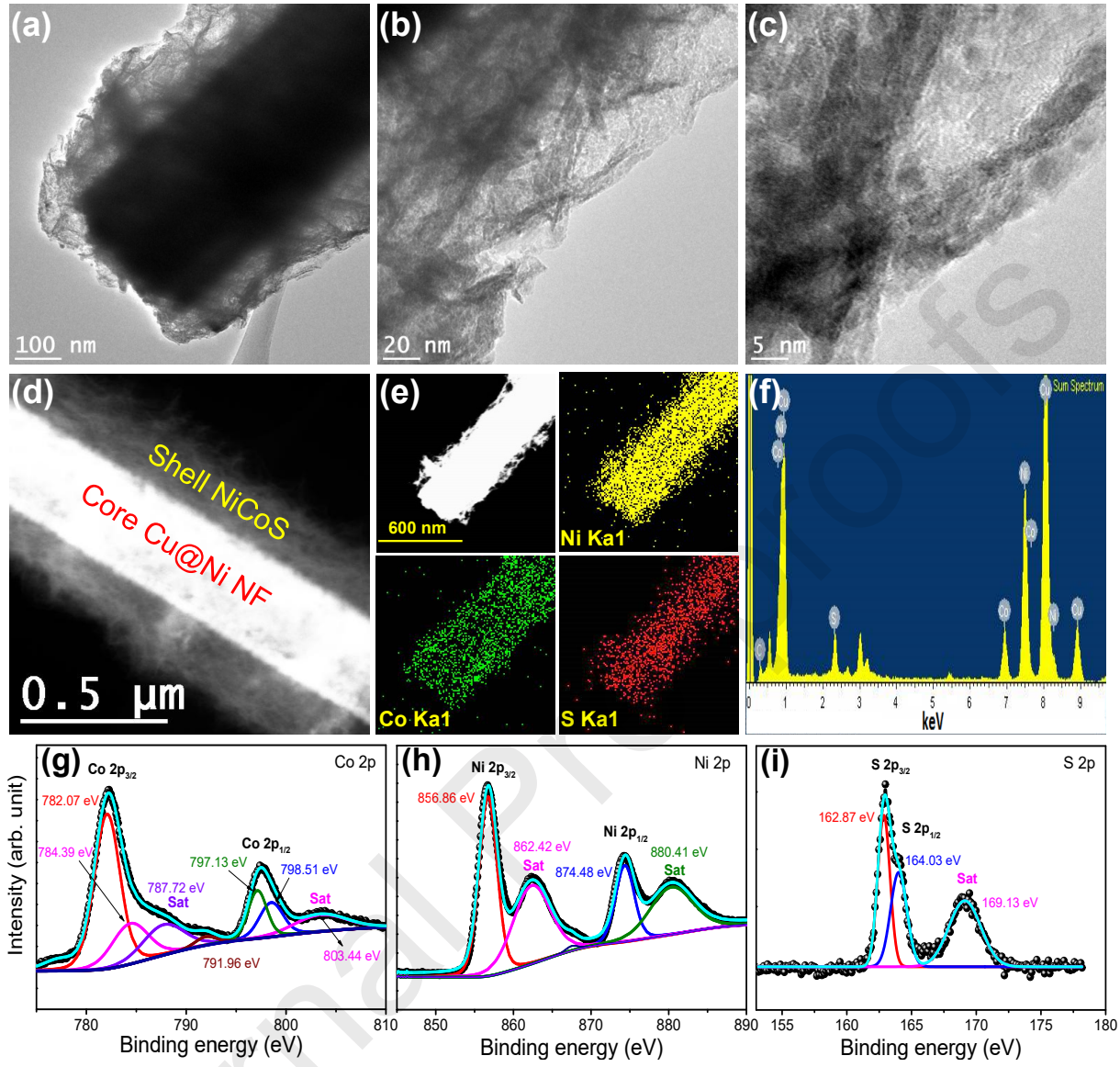

Fig. 3. (a-c) Typical TEM images of intertwined nanosheet Cu@Ni@NiCoS NFs core-shell network electrode at different magnifications. (d) HAADF-STEM image showing a contrast difference between the Cu@Ni NF core and the NiCoS shell. (e) HAADF-STEM -EDX mapping of the Cu@Ni@NiCoS NF, demonstrating the homogeneous distribution of Ni, Co, and S elements over the Cu@Ni NF. (f) EDX spectra of Cu@Ni@NiCoS NF. (g-i) High -resolution XPS spectra of Co 2p, Ni 2p, and S 2p, respectively.

difference between the core Cu@Ni NFs (bright) and the shell NiCoS nanosheet (dark), further signifying the formation of the core-shell network structure of Cu@Ni@NiCoS NFs, agreeing with FE-SEM photographs presented in Fig. 2e and 2f. In addition, we performed HAAD-STEM-EDX mapping to further analyze the uniform growth of NiCoS nanosheet and the elemental distribution of Ni, Co, and S over the core Cu@Ni NFs network (Fig. 3e). STEM-EDX mapping images of Ni, Co, and S correspond to K-edge signals and a homogeneous Ni, Co, and S elemental distribution were observed, suggesting uniform electrodeposition of the intertwined NiCoS nanosheet over the Cu@Ni NFs (Fig. S6). The selected area EDX spectra shown in Fig. 3f also indicated the presence of constituent elements.

The valence state and chemical composition of the NiCoS nanosheet over the Cu@Ni NFs was further studied using XPS (X-ray photoelectron spectroscopy). (Fig. S7) illustrates the survey XPS spectrum of Cu@Ni@NiCoS NFs network electrode and confirmed the presence of Ni, Co, and Sas the constituent elements, in agreement with the elemental HAADF-STEM -EDX color mapping and EDX spectra (Fig.3e-f).With a Gaussian fitting method, high-resolution XPS spectra of Co 2p, Ni 2p, and S 2p core levels were obtained and are shown in Fig. 3g, 3h, and 3i, respectively. The fitted Co 2p spectrum (Fig. 3g) displayed two spin-orbit doublets centered at 797.4 and 782.2 eV which corresponded to Co $2p_{1/2}$ and Co $2p_{3/2}$, respectively, and two satellite peaks at 787.7 and 803.4 eV, respectively [56]. The presence of two pairs of doublet peaks demonstrated the presence of two different cobalt oxidation valence states: Co^{2+} and Co^{3+}[56–58]. The fitted Ni 2p spectrum (Fig. 3h) also showed two spin-orbit doublets at 874.3 and 856.6 eV matching to Ni $2p_{1/2}$ and Ni $2p_{3/2}$, respectively, along with two satellite peaks at 880.4 and 862.3 eV, respectively. These pairs of doublet peaks indicated the presence of both Ni^{2+} and Ni^{3+} oxidation states [59,60].The results of XPS analysis of the two metal elements in NiCoS showed

the existence of various valence states of Co and Ni, which in turn might improve the electrochemical performance by multiple redox reactions [35,60]. For the S 2p spectrum (Fig. 3i), the fitted S 2p showed one satellite peak and one main peak. The main peak could be de-convoluted into two peaks centered at a binding energy of 163.9 and 162.8 eV corresponding to S $2p_{1/2}$ and S $2p_{3/2}$, respectively. They were assigned to metal-sulfur bonds (Co-S and Ni-Sbonds) in the ternary NiCoS [35,60,61]. The satellite peak noted at higher binding energy 168.5 eV could be ascribed to sulfur ion oxidation at the surface with a higher oxide state [62,63]. Furthermore, the crystal phase of the Cu@Ni@NiCoS NFs network electrode was characterized by measuring the X-ray diffraction pattern of the sample, Fig. S8.Due to the high-intensity peak arising from the substrate, the XRD pattern of the active NiCoS material is also shown in the enlarged portion of the pattern in the inset of Fig.S8. The XRD pattern exhibits the formation of the cubic phase structure of nickel cobalt sulfide ($NiCo_2S_4$) with three noticeable main peaks at 2θ values of 38.19°, 46.9 and 55.1° respectively which are assigned to the (400), (422), and (440) planes of the $NiCo_2S_4$ (ICDD card No. 00-043-1477) [43, 58]. The peaks corresponding to 2θ values of 43.4° and 50.6° were assigned to the (111) and (200) planes of Copper (ICDD card No. 00-001-1242), respectively while the peak at 44.6° assigns to (111) plane of Nickel (ICDD card No.00-001-1260), which arises from the Cu@Ni core.

In our previous report [51], we have already highlighted that the electro-optical performance of the electrospun nanofiber-based metal network electrode can be simply tuned or varied by just controlling the electrospinning time. Fig. 4a displays optical transmittance spectra of the bare Cu@Ni NFs network electrode in comparison with NiCoS nanosheets having different electrodeposition time. The bare Cu@Ni NFs network electrode showed a high opto-electrical performance (~89 % transmittance with 12.19 Ω/sq sheet resistance). It was observed that the

optical transparency of the Cu@Ni@NiCoS NFs network electrode decreases with an increase in the electrodeposition time. The decrease in transmittance % of the electrode with deposition time might be attributed to the increase in Cu@Ni@NiCoS NFs size as well as the increase in partial growths over the PEN film as suggested by FE-SEM photographs shown in Fig. S9. Compared to the bare Cu@Ni NFs network electrode (~90 % T), a maximum optical loss of ~34 % (~56 % T) and a minimum of 5% loss (~85 % T) were observed for 60 min and 10 min electrodeposited electrode samples, respectively. The high transparency in our Cu@Ni@NiCoS NFs network electrode might arise from the selective growth of NiCoS nanosheet only over the surface of the core Cu@Ni NFs resulting in the formation of the large open area by the network, as illustrated in the FE-SEM photograph Fig. 2d [7].A digital photograph of the Cu@Ni@NiCoS NFs network electrodes with different deposition time is shown in Fig. 4b, signifying the high transparency of the electrodes. These electrodes became darker as the deposition time increased. Electro-mechanical bending properties of the electrodeposited Cu@Ni@NiCoS NFs network electrodes on PEN substrates were also studied. Fig. S10a showed an almost negligible change in resistance under different bending radii. Again, the electrodes also showed outstanding long-term bending cycling properties, with only a ~5 % increase in resistance percentage after 10,000 repeated cycles at a 3.0 mm radius, Fig. S10b.To further confirm the mechanical flexibility of the electrode, the SEM photographs of the electrode were measured under the bending condition as shown in Fig S10c,d. The FE-SEM photographs showed that even at bending conditions, the electrode material was strongly and evenly bonded to the PEN substrate and no crack or break of the nanofibers networks were observed, which indicates the structural robustness of our electrode materials even under bending process. Fig S10e shows the digital photographs of the electrode sample at different bending radii. We also check the electrochemical performance of the electrode sample before and

after 10,000 repeated cycles at a 3.0 mm radius. Fig S11b shows the CV curves of the Cu@Ni@NiCoS NFs network electrode measured before and after 10,000 bending cycles at 3 mm bending radius, at a scan rate of 10 mV/s. The electrode showed a decrease of ~7% areal capacitance (mF/cm^2) after repeated 10,000 bending cycles demonstrating its excellent mechanical flexibility.

Fig. 4c displays CV curves of the Cu@Ni@NiCoS NFs network electrode samples with different electrodeposition time at 10 mV/s scan rate. It is noticeable that as the deposition time increases the area of the CV loop as well as the current density of the redox peak increases rapidly. It then decreased after 50 min of electrodeposition, suggesting that the optimum deposition time or maximum mass loading capability of the NiCoS over the Cu@Ni NFs was 50 min. Areal capacities of the Cu@Ni@NiCoS NFs network electrodes were then calculated using (Eq. S1). Fig. 4d shows a graph of the optical transparency and areal capacity of the Cu@Ni@NiCoS NFs network electrodes as a function of electrodeposition time. As deposition time increased, the optical transparency of the electrode sample decreased steadily while the areal capacity increased rapidly up to a peak value and then decreased with further increase in time. It was significant that optical and areal capacities of the Cu@Ni@NiCoS NFs network electrode could be tuned in a wide range by simply controlling the electrodeposition time. By sacrificing the transparency of the electrode, a high areal capacity of ~9.73 μA h/cm^2 could be achieved at ~64.12 % transmittance. It is apparent that with increasing electrodeposition time the size and thickness of the nanosheet become obviously bigger and thicker as suggested by FE-SEM photographs of Cu@Ni@NiCoS NFs for different deposition time, Fig. S9. Formation of large cracks was observed and also the network electrodes were broken at junction points due to over deposition and larger mechanical expansion for the sample with 60 min of deposition

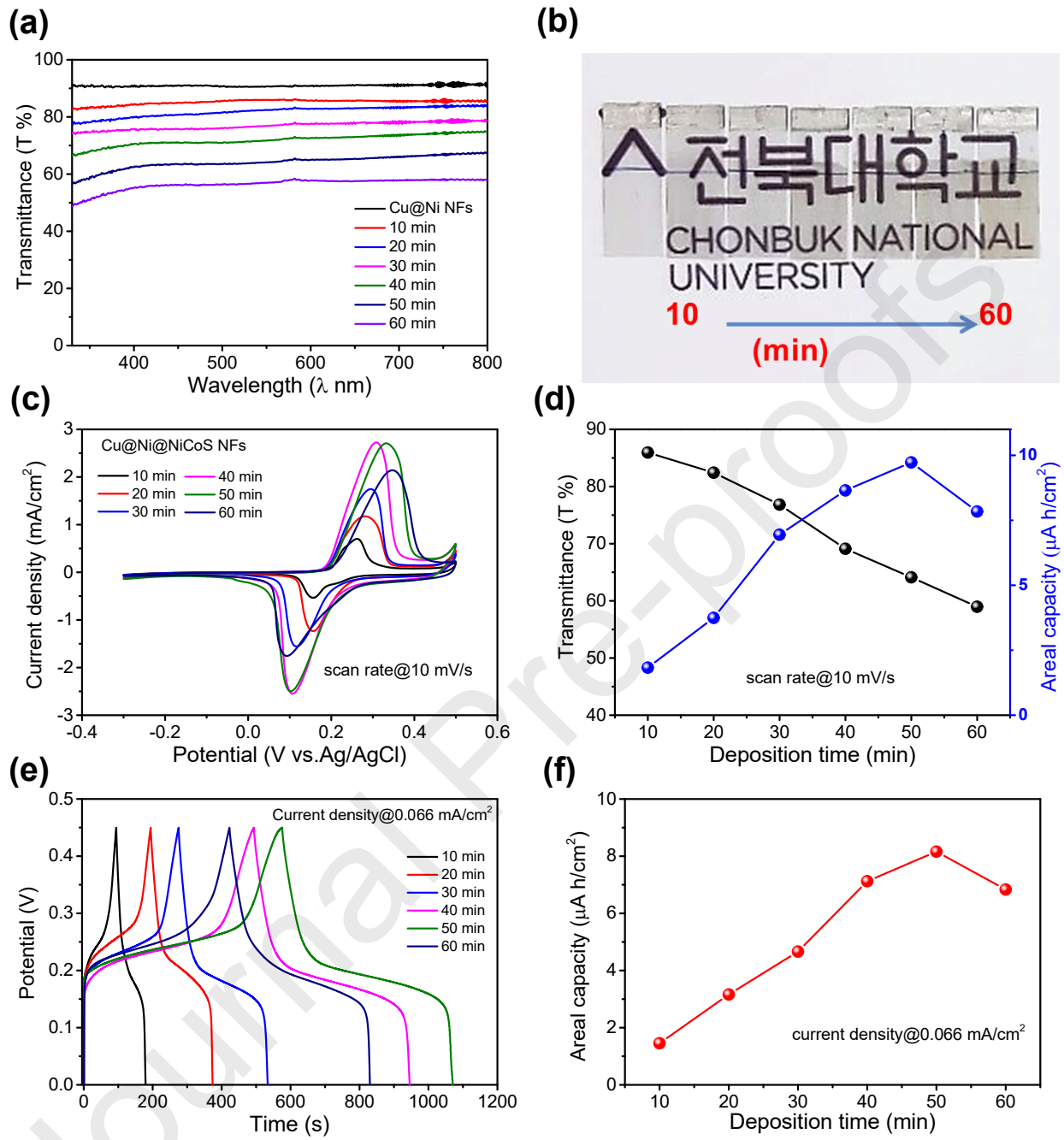

Fig. 4. (a) Optical transparency spectra of the bare Cu@Ni NFs network and Cu@Ni@NiCoS NFs network electrodes with different electrodeposition time. (b) Digital photographs of Cu@Ni NFs and Cu@Ni@NiCoS NFs network electrodes on PEN substrate with different electrodeposition time. (c) Cyclic voltammogram (CV) curves of Cu@Ni@NiCoS NFs network electrodes with

different electrodeposition time at a scan rate of 10 mV/s. (d) Optical transmittance (%) and areal capacity of the Cu@Ni@NiCoS NFs network electrodes determined from CV curves with respect to electrodeposition time. (e) GCD curves of Cu@Ni@NiCoS NFs network electrodes with different electrodeposition time at a current density of 0.066 mA/cm^2. (f) Areal capacity determined from the GCD curve (Fig. 4e) as a function of electrodeposition time.

(Fig. S9 c,f). Thus, the formation of thicker, denser and large cracks might lead to a decrease in the electrical conductivity, porous structure, and redox-active sites, resulting to fall in the electrochemical performance of the supercapacitor electrode as observed in Fig. 4d [6,7].Fig. 4e shows GCD curves of different Cu@Ni@NiCoS NFs network electrodes at various electrodeposition times. All electrodes showed similar charge-discharge characteristics. However, the sample with 50 min of electrodeposition showed higher discharge time (~501 s) than other samples, indicating its higher areal capacity. Specific capacities (μAh/cm^2) of the Cu@Ni@NiCoS NFs network electrodes were also evaluated from the GCD curvesusing (Eq. S3), shown in Fig. 4f. The electrode sample with 50 min of electrodeposition showed a high specific capacity of ~8.16 μA h/cm^2 whereas the sample with 10 min deposition showed the lowest specific capacity of 1.45 μA h/cm^2. Based on the above experimental observations such as transparency and areal capacity results, we found that the optimized deposition time of NiCoS on Cu@Ni NFs network was 30 min, demonstrating high transparency of ~76.83 % with a high areal capacity of ~6.94 μA h/cm^2 at 10 mV/s.

Next, we examined the electrochemical performance of the optimized Cu@Ni@NiCoS NFs network electrode (30 min) as a battery-type supercapacitor electrode for fabricating high energy density transparent flexible SSC devices. Fig. 5a displays characteristic CV curves of the

Cu@Ni@NiCoS NFs network electrode measured in -0.3 to +0.5 V potential window, with Ag/AgCl electrode as a reference electrode, under various scan rate.Note that the bareCu@Ni NFs network electrode contributes a negligible current density in the observed large CV loop of the Cu@Ni@NiCoS NFs network electrode (Fig. S11a). It is significant that the Cu@Ni@NiCoS NFs network electrode displayed a pair of redox peaks, representing the occurrence of the Faradic redox reaction of the NiCoS active material during the electrochemical reaction. It is well known that for battery-type supercapacitor electrodes, their CV curves display sharp and high current redox peaks due to the fast-Faradic process while in the case of EDLCs, the CV loop displays nearly rectangular shape. The existence of the redox peaks might result from surface Faradic redox reactions associated with the redox behavior of Co^{2+}/Co^{3+} and Ni^{2+}/Ni^{3+} couples. The existence of redox peaks might attribute to thereversible electrochemical redox reaction behavior of battery-type electrode materials with alkaline electrolyte in agreement with previous studies:[40,41]

$$CoS + OH^- \leftrightarrow CoSOH + e^-;$$

$$CoSOH + OH^- \leftrightarrow CoSO + H_2O + e^-;$$

$$NiS + OH^- \leftrightarrow NiSOH + e^-;$$

$$NiSOH + OH^- \leftrightarrow NiSO + H_2O + e^-$$

Also, the Cu@Ni@NiCoS NFs network electrode showed symmetric anodic and cathodic peak, signifying the high reversibility of the ternary NiCoS nanosheet electrode. Again, with the increase in the scan rate from 5 to 100 mV/s, it is observed that the anodic peaks shiftstoward higher potentials while cathodic peaks toward lower potentials owing to the electrode's internal resistance and the polarization effect [64]. In addition, the Cu@Ni@NiCoS NFs network electrode displayed

a good linear relationship for both cathodic and anodic peaks with a scan rate (Fig. 5b). This result specifies its good reversibility and high rate capability owing to the fast ionic/diffusion rate, in good agreement with previous reports [65–67]. Fig. 5c shows GCD curves of the Cu@Ni@NiCoS NFs network electrode (-0.1 to +0.45 V *vs.* Ag/AgCl) measured at different applied current densities (0.04 to 5 mA/cm^2). It is observed that the electrode exhibited almost symmetric characteristics, indicating excellent Coulombic efficiency, which might be due to highly reversible redox reactions during the GCD cycle. Additionally, GCD curves showed well-defined voltage plateaus at 0.20–0.27 V for charging and 0.14-0.21 V for discharging, revealing its high pseudo-capacitive behavior. This indicates dominant diffusion-controlled kinetics in the Cu@Ni@NiCoS NFs network electrode [43]. The characteristic voltage plateau in the GCD might have originated from the charge transfer process that occurs at the electrolyte-electrode interface. Also, the negligible IR drop in the GCD curve showed exceptional rate capability, good electrical and ionic conductivity. Fig. 5d shows the calculated areal capacities of the Cu@Ni@NiCoS NFs network electrode with respect to scan rates and current densities, respectively. Calculated areal capacities of the electrode determined from the CV and GCD curves were almost comparable. They were as high as 7.43 μA h/cm^2 at a scan rate of 5 mV/s and as low as 4.24 μA h/cm^2 at 100 mV/s scan rate (Fig. 5d, above) with retention of ~70 % areal capacity. The high areal capacity retention suggests a high rate performance of the Cu@Ni@NiCoS NFs network electrode. Similarly, areal capacities measured from the GCD curves were found to be decreased from 4.78 μA h/cm^2 to 3.76 μA h/cm^2 as the applied current densities increases from 0.04 mA/cm^2 to 5 mA/cm^2, respectively (Fig. 5d, below), suggesting an areal capacity retention of ~79 %, demonstrating the excellent rate capability of the electrode.

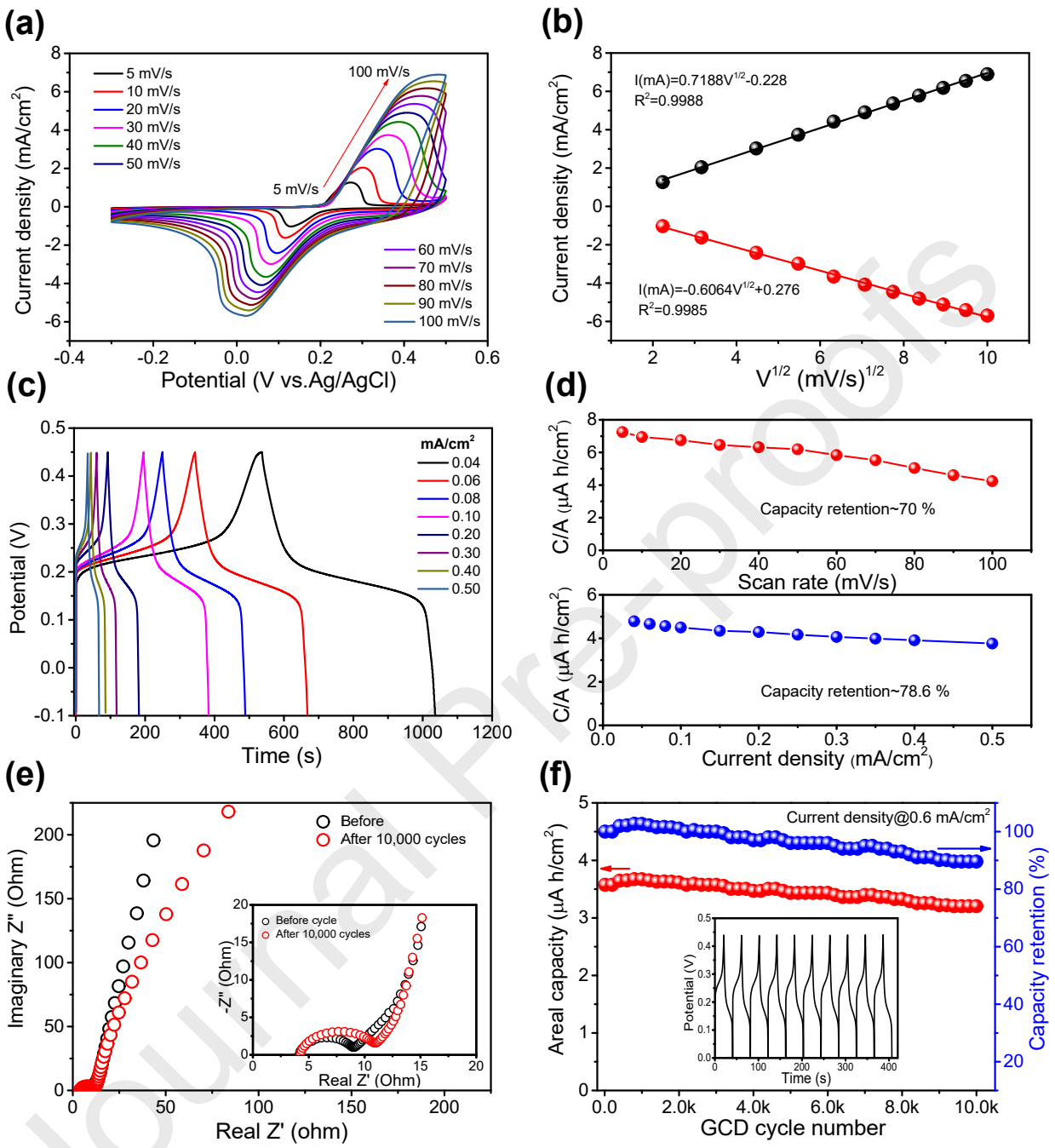

Fig. 5. Electrochemical measurements of Cu@Ni@NiCoS NFs network supercapacitor electrode in a three-electrode system using 2 M KOH electrolyte solution. (a) CV curves measured at different scan rates of 5-100 mV/s. (b) A linear relationship of redox peak current vs. square root of scan rate. (c) Charge-discharge (GCD) curves of the electrode under different current densities.

(d) Areal capacity (μA h/cm^2) as a function of scan rate (mV/s) and current density (mA/cm^2) determined from CV and GCD curves (Figs. 5a and 5c). (e) EIS impedance spectra of the electrode measured in the range of 0.01 Hz to 100 kHz frequency. (f) Long-term cycling stability performance of the electrode measured at an applied current density of 0.6 mA/cm^2. (inset: 1st 10 GCD cycles of the electrode).

Electrochemical impedance spectroscopy (EIS) study is one useful technique to study the electrochemical performance of the supercapacitor electrode. Fig. 5e shows EIS (Nyquist) plots of the Cu@Ni@NiCoS NFs network electrode measured in the range of 0.01 Hz to 100kHz frequency. The EIS spectra exhibited a small semi-circle and a nearly vertical straight line in the high and low-frequency ranges, respectively (inset: enlarged EIS spectra in the high-frequency region). The evaluated charge transfer resistance (R_{ct}) and the bulk solution resistance (R_s) of the electrode were found to be 9.15Ω and 4.13 Ω, respectively. Notably, the low R_s and R_{ct} of the Cu@Ni@NiCoS NFs network electrode revealed high ionic conductivity and low charge-transfer resistance of the electrode, respectively, which could enable fast electron transfer and redox reaction. These results of electrochemical performances reveal that the Cu@Ni@NiCoS NFs network electrode possesses low impedance with excellent charge capacity. In addition, the electrochemical stability of the electrode in an alkaline electrolyte is necessary for commercial applications of supercapacitors and batteries. To test the stability of the Cu@Ni@NiCoS NFs network electrode in alkaline electrolyte, repeated charge-discharge cyclic test was conducted in a 50 ml of 2 M KOH solution at 0.6 mA/cm^2(current density) for 10,000 cycles,Fig. 5f. Notably, after the 10,000 GCD cycles, the electrode showed ~89% capacity retention, signifying good cycling stability. The long-life cyclic stability with high capacity of the electrode might have originated from the hierarchical interconnected wrinkle nanosheets structure of the NiCoS directly grown over the conducting

Cu@Ni NFs framework. The direct growth of conductive NiCoS over the Cu@Ni NFs formed an integrated electrode structure that allowed fast electron transportation between Cu@Ni NFs current collector and the active NiCoS nanosheet [6,7]. Again, the nanoporous structure of the interconnected wrinkle NiCoS nanosheets along with large open areas of the Cu@Ni@NiCoS NFs network framework might offer a large specific surface area that allows simplistic electrolyte ion transportations and enhances fast and reversible redox reactions, thus greatly improving the rate capability and adding to the large charge storage capacity. The EIS of the Cu@Ni@NiCoS NFs network electrode was also measured after 10,000 GCD cycles to further check the electrode's stability. The results are displayed in Fig. 5e in comparison with EIS measured before the cyclic test. There was a small variation in the high-frequency region with a small increase in the radius of the semi-circle, suggesting a small increase in the charge-transfer resistance after 10,000 GCD cycles. There was a slight deviation in the vertical line of the low-frequency region, although the bulk solution resistance remained almost constant, demonstrating the high cyclingelectrode's stability.Again, the electrochemical performance at high transparency of the Cu@Ni@NiCoS NFs network battery type supercapacitorelectrode demonstrated better performance in comparison to those of the previous reported transparent flexible supercapacitors; MnO_2@AuNFs[7], metal network/MnO_2[12], Au@MnO_2 [31], MnO_2/ITO/PET [32], $Co(OH)_2$/AgNWs [33], AgNW@NiCo/$NiCo(OH)_2$ [25], and metal nanowires/metal oxide [68].

To explore the practical application of a flexible, transparent, and lightweight solid-state supercapacitor (SSC) device as a portable power source, we fabricated a flexible and transparent solid-state SCs device as shown in the scheme 1. Herein, Cu@Ni@NiCoS NFs network supercapacitor electrodes acted as both negative and positive electrodes with PVA-KOH gel as an electrolyte. It is expected that owing to the high mechanical flexibility of PVA-KOH gel

electrolytemight also improve mechanical flexible properties of the fabricated SSC device where it acts asboth a binder and an electrolyte. The optical transparency of the fabricated SSC device in comparison with that of the single Cu@Ni@NiCoS NFs network electrode is displayed in Fig. 6a. The transparent flexibleSSC device exhibited high optical transparency of ~65 % at 550 nm wavelength with a ~10 % loss in transparency compared to the single Cu@Ni@NiCoS NFs network electrode and almost comparable with those of the transparent supercapacitor devices reported [7,12,30-33,68]. A digital image of the fabricated SSC device is presented in Fig. 6a (inset), representing its good transparency. The high optical transparency of the SSC device might be ascribed to the high transparency of the Cu@Ni@NiCoS NFs network (~77 %) and the PVA-KOH gel electrolyte. The electrochemical properties of the fabricated SC device were then characterized in a two-electrode configuration method. Fig. 6b shows characteristic CV profiles of the transparent flexible SSC device measured at the potential of 0.0 to 0.8 V under different scan rates (10 mV/s to 100mV/s). It was observed that even at a scan rate of 2 V/s, the device maintained its characteristic CV, indicating its low contact resistance, excellent rate capabilities, andhigh capacitive performance (Fig. S12a). The galvanometric charge-discharge (GCD) characteristic of the transparent flexible SSC device was also measured under various current densities in the range of 0.02 to 0.075 mA/cm^2 with the potential of 0 to 0.8 V, Fig. 6c. The SSC device exhibited almost symmetric GCD features with a negligible voltage drop (IR drop) at various current densities, demonstrating a good capacitive characteristic of the device. Areal capacities of the transparent flexible SSC device were calculated from its characteristic CV and GCD curves using (Eq. S4 and S5). Fig. 6d displayed the calculated areal capacities of the device with respect to scan rate (above) and current densities (below). The transparent flexible SSC device showed almost comparable areal capacities calculated from the two approaches, exhibiting a high capacity of ~1.51μA h/cm^2

at 10 mV/s which decreases to 0.74 μA h/cm^2 at 100 mV/s (Fig. 6d, above). The device retained almost ~50 % of the initial areal capacity;when the scan rate was increased from 10 mV/s to 100 mV/s, demonstrating a high rate capability of the device. Areal capacities measured from the GCD curves were found to be 1.21, 0.98, 0.85, 0.75, 0.67, 0.59, 0.52, 0.47, 0.43, 0.39, and 0.37 μA h/cm^2 at applied current densities of 0.025, 0.03, 0.035, 0.04, 0.045, 0.05, 0.055, 0.06, 0.065, 0.07, and 0.075 mA/cm^2, respectively (Fig. 6d, below). The symmetric GCD curves of the transparent flexible SSC device also suggested an excellent Coulombic efficiency. One important parameter that signifies the overall electrochemical performances of the transparent flexible SC device is its long life GCD cycle stability. The long-term charge-discharge stability of the SSC device was investigated by performing continuous 10,000 GCD cycles at a constant current density of 0.075 mA/cm^2, Fig. 6e. The SSC device exhibited excellent long-term cycle stability and retained almost ~92% of its initial capacity, demonstrating the good structural integrity of the Cu@Ni@NiCoS NFs network electrode. Compared to the single electrode, the SSC device showed higher stability possibly due to the solid gel electrolyte. The decrease in the capacity of the device after long-term cycles might be due to partial change of ternary sulfide to oxide or hydroxide, delamination/dissolution of a small portion of NiCoS nanosheet from the electrode caused by volume expansion, or slight morphological damage [44]. Also, the transparent flexible SSC device maintained almost 99%

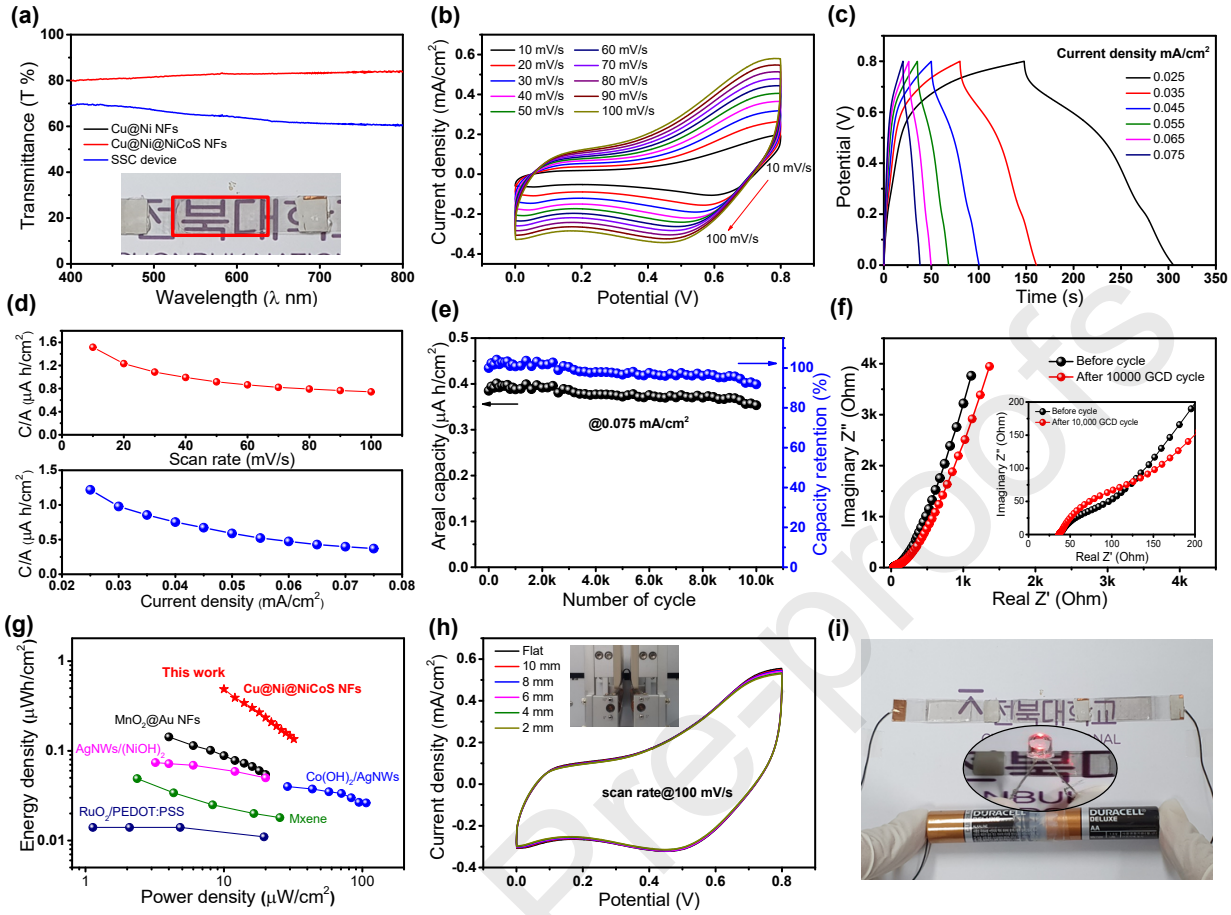

Fig. 6. (a) Transparency spectra of Cu@Ni NFs, Cu@Ni@NiCoS NFs, and the SSC device fabricated using two Cu@Ni@NiCoS NFs network electrodes (inset: digital image of the SSC device demonstrating its high transparency). (b) CV curves of the flexible transparent SSC device measured at various scan rates of 10 mV/s-100 mV/s. (c) GCD curves of the flexible transparent SSC device at various current densities. (d) Areal capacity (μA h/cm^2) of the SSC measured device as a function of scan rate and current density. (e) Long-term GCD stability tests of the SSC device with 10000 cycles at 0.075 mA/cm^2. (f) EIS spectra (Nyquist plots) of the flexible transparent SSC device measured before and after long-term cycling stability. (g) Energy density vs. power density graph (Ragone plot) of the transparent flexible SSC device in comparison with previously reported transparent devices. (h) Mechanical bending test of the SSC device by measuring the characteristic CV of the SSC device at various bending radii at a scan rate of 100 mV/s (inset: digital image of

flexible transparent SSC device, showing its high mechanical bending ability). (i) Digital image of charging a three-SSC device (connected in series) with two 1.5 V AA battery, connected in series for 15 sec (inset lighting a red LED bulb after charging for 15 sec).

Coulombic efficiency after 10,000 GCD cycles, as suggested by 1st 10 cycles and last 10 cycles, as shown in Fig. S12c,d. The ac impedance spectra (EIS) of the SSC device were also characterized in the range of 0.1 Hz to 100 kHz frequency (Fig. 6f). The EIS spectra (Nyquist plots) illustrated R_s~37.39 Ω and R_{ct}~ 89.33 Ω, respectively before the cyclic stability test. After 10,000 GCD cycles test, R_s and R_{ct} were found to be 40.64 Ω and 109.79 Ω, respectively, showing a slight increase in resistance which demonstrated the long-term cyclic stability of the device. A slight deviation in the straight line of the low-frequency region was also observed after 10,000 CGD cycles. Fig. 6g shows the Ragone plot of the transparent flexible SSC device determined from discharge curves. Accordingly, our transparent flexible SSC device showed a high area energy density of ~0.48 μW h/cm^{2}with a power density of 11.16 μW/cm^2. The Cu@Ni@NiCoS NFs based transparent flexible SSC devices demonstrated better energy and power densities from those of earlier reported transparent supercapacitor devices such as MnO_2@AuNFs [7], RuO_2/PEDOT:PSS [20], $Co(OH)_2$/AgNWs [33], AgNWs/$Ni(OH)_2$/PEDOT:PSS [68], MXene [69], and graphene quantum-dot [70]. Power densities and energy densities of the flexible transparent supercapacitor device in comparison with those of previous transparent flexible supercapacitors are highlighted in (Table S2). For industrial aspects, volumetric energy and power densities are the main factors for SSC devices. Thus, volumetric capacity, power, and energy densities of the SSC device were also evaluated from the discharge curves of the device by measuring the thickness of the device (subtracting the thickness of the two PEN substrate). They were found to be as high as ~27.06 μA

h/cm^3 at a volumetric current density of 0.55 mA/cm^3, respectively (Fig. S12e). The transparent flexible SSC device also displays a high volumetric energy density of 10.83 μW h/cm^3 at a volumetric power density of 248 μW/cm^3 (Fig. S12f). For flexible and transparent device applications, the transparent SSC device should also have high mechanical flexibility. Thus, the mechanical properties of the SSC device were also determined by measuring the cyclic voltammetry (CV) curves of the SSC device under different mechanical bending radii. The results are shown in Fig. 6h (inset, a digital image of a bending SSC device). Fig. 6h shows characteristic CV curves of the SSC device measured under mechanical bending at the scan rate of 100 mV/s. The SSC device demonstrated excellent mechanical flexibility. An almost negligible change in CV curves was observed even up to a bending radius of 2 mm. All CV curves almost overlapped to each other, suggesting a negligible degradation in the capacitive property of the SSC device. This demonstrates the high mechanical bending property of the fabricated transparent flexible SSC device. Fig. S13a-c shows the digital photographs of the flexible transparent SSC device bending at different angles demonstrating its high bending capability. Fig. 6i demonstrates the practical application of the transparent flexible SSC device, where three similar SSC devices were connected in series to light a RED LED bulb (Fig. S13d-f). From the above results of optical, electrochemical, and mechanical performance of the Cu@Ni@NiCoS NFs network single electrode and the fabricated SSC device, it is proposed that the core-shell Cu@Ni@NiCoS NFs network electrode might be a superior transparent flexible supercapacitor electrode for application of next-generation transparent flexible energy storage devices because of their high electrochemical performance at high transparency along with excellent mechanical flexibility. It is proposed that the electrochemical performance of the transparent supercapacitor electrode might be improved further with proper choice of active materials using the direct growth technique which

limits the growth of active materials only over the metal nanofiber backbone, leaving behind large open areas for high transmission of light.

4. Conclusion

We successfully fabricated a transparent flexible ternary metal sulfide@metal nanofibers network electrode as an efficient battery type supercapacitor electrode via simple electrospinning, physical deposition and electrodeposition techniques. In particular, a highly flexible, transparent and chemically stable Cu@Ni NFs network was fabricated using a combined technique of electrospinning and physical deposition process. The Cu@Ni NFs network electrode displayed a high electro-optical property (sheet resistance~12.19 Ω/sq at ~89 % transmittance). With chemically stable Cu@Ni NFs network as the backbone and using a simple electrodeposition technique, hierarchal intertwined ternary NiCoS nanosheets were successfully grown over the Cu@Ni NFs network, resulting to a formation of core-shell Cu@Ni@NiCoS NFs network structure. Again, with the high porous interconnected nanosheet structure of the shell along with the nanofiber network structure of the Cu@Ni@NiCoS NFs electrode largely enhanced the electrochemical performance at high transparency. The core-shell Cu@Ni@NiCoS NFs network electrode revealed an excellent areal capacity of 7.43 μA h/cm^2 at a scan rate of 5 mV/s with high transparency of ~76.83%. Moreover, the assembled transparent flexible SSC device showed high areal capacity of 1.21μA h/cm^2 at an applied current density of 0.025 mA/cm^2 with transparency of ~65%. The SSC device also demonstrated a high volumetric capacity of 24.35 μA h/cm^3, a high energy density of 0.48 μW h/cm^2 at a power density of 11.16 μW/cm^2, a long-term GCD stability (~92% retention of its initial areal capacity after 10,000 GCD cycles), and excellent mechanical flexibility. Thus, the present work offers a scalable and simple method to fabricate a ternary metal

sulfide@metal nanofiber network electrode with suitable stoichiometric for next-generation transparent flexible energy storage applications.

Acknowledgments

This research was supported by the Basic Research Laboratory Program (2014R1A4A1008140), Nano-Material Technology Development Program (2016M3A7B4900117), and Basic Science Research Program (2017R1A2B3004917) through the National Research Foundation (NRF) funded by the Ministry of Science and ICT, Republic of Korea.

Appendix A. Supplementary data

References

[1] D. Li, X. Liu, X. Chen, W.Y. Lai, W. Huang, A Simple Strategy towards Highly Conductive Silver-Nanowire Inks for Screen-Printed Flexible Transparent Conductive Films and Wearable Energy-Storage Devices, Adv. Mater. Technol. 4 (2019) 1–7. doi:10.1002/admt.201900196.

[2] T. Cheng, Y.W. Wu, Y.L. Chen, Y.Z. Zhang, W.Y. Lai, W. Huang, Inkjet-Printed High-Performance Flexible Micro-Supercapacitors with Porous Nanofiber-Like Electrode Structures, Small. 15 (2019) 1–9. doi:10.1002/smll.201901830.

[3] Y.Z. Zhang, Y. Wang, T. Cheng, L.Q. Yao, X. Li, W.Y. Lai, W. Huang, Printed supercapacitors: Materials, printing and applications, Chem. Soc. Rev. 48 (2019) 3229–3264. doi:10.1039/c7cs00819h.

[4] D. Li, W.Y. Lai, Y.Z. Zhang, W. Huang, Printable Transparent Conductive Films for Flexible Electronics, Adv. Mater. 30 (2018) 1–24. doi:10.1002/adma.201704738.

[5] T. An, W. Cheng, Recent progress in stretchable supercapacitors, J. Mater. Chem. A. 6 (2018) 15478–15494. doi:10.1039/c8ta03988g.

[6] Y.H. Liu, J.L. Xu, X. Gao, Y.L. Sun, J.J. Lv, S. Shen, L. Sen Chen, S.D. Wang, Freestanding transparent metallic network based ultrathin, foldable and designable supercapacitors, Energy Environ. Sci. 10 (2017) 2534–2543. doi:10.1039/c7ee02390a.

[7] S.B. Singh, T.I. Singh, N.H. Kim, J.H. Lee, A core-shell MnO_2@Au nanofiber network as a high-performance flexible transparent supercapacitor electrode, J. Mater. Chem. A. 7 (2019) 10672–10683. doi:10.1039/c9ta00778d.

[8] P. Simon, Y. Gogotsi, Materials for electrochemical capacitors, Nature Materials 7 (2008) 845–854.

[9] C. Zhang, Y. Xie, M. Zhao, A.E. Pentecost, Z. Ling, J. Wang, D. Long, L. Ling, W. Qiao, Enhanced electrochemical performance of hydrous RuO_2/mesoporous carbon nanocomposites via nitrogen doping, ACS Appl. Mater. Interfaces. 6 (2014) 9751–9759. doi:10.1021/am502173x.

[10] X.Y. Liu, Y.Q. Gao, G.W. Yang, A flexible, transparent and super-long-life supercapacitor based on ultrafine Co_3O_4 nanocrystal electrodes, Nanoscale. 8 (2016) 4227–4235. doi:10.1039/c5nr09145d.

[11] M.A. Borysiewicz, M. Ekielski, Z. Ogorzałek, M. Wzorek, J. Kaczmarski, T. Wojciechowski, Highly transparent supercapacitors based on ZnO/MnO_2 nanostructures, Nanoscale. 9 (2017) 7577–7587. doi:10.1039/c7nr01320e.

[12] S. Kiruthika, C. Sow, G.U. Kulkarni, Transparent and Flexible Supercapacitors with Networked Electrodes, Small. 13 (2017) 1–9. doi:10.1002/smll.201701906.

[13] N. Li, G. Yang, Y. Sun, H. Song, H. Cui, G. Yang, C. Wang, Free-standing and transparent graphene membrane of polyhedron box-shaped basic building units directly grown using a NaCl template for flexible transparent and stretchable solid-state supercapacitors, Nano Lett. 15 (2015) 3195–3203. doi:10.1021/acs.nanolett.5b00364.

[14] N. Li, X. Huang, H. Zhang, Y. Li, C. Wang, Transparent and Self-Supporting Graphene Films with Wrinkled- Graphene-Wall-Assembled Opening Polyhedron Building Blocks for High Performance Flexible/Transparent Supercapacitors, ACS Appl. Mater. Interfaces. 9 (2017) 9763–9771. doi:10.1021/acsami.7b00487.

[15] C.S. Lee, J.E. Yoo, K. Shin, C.O. Park, J. Bae, Carbon nanotube-silver nanowire composite networks on flexible substrates: High reliability and application for supercapacitor electrodes, Phys. Status Solidi Appl. Mater. Sci. 211 (2014) 2890–2897. doi:10.1002/pssa.201431538.

[16] D.S. Hecht, L. Hu, G. Irvin, Emerging transparent electrodes based on thin films of carbon nanotubes, graphene, and metallic nanostructures, Adv. Mater. 23 (2011) 1482–1513. doi:10.1002/adma.201003188.

[17] Z. Niu, W. Zhou, J. Chen, G. Feng, H. Li, Y. Hu, W. Ma, H. Dong, J. Li, S. Xie, A repeated halving approach to fabricate ultrathin single-walled carbon nanotube films for transparent supercapacitors, Small. 9 (2013) 518–524. doi:10.1002/smll.201201587.

[18] T.M. Higgins, J.N. Coleman, Avoiding Resistance Limitations in High-Performance Transparent Supercapacitor Electrodes Based on Large-Area, High-Conductivity

PEDOT:PSS Films, ACS Appl. Mater. Interfaces. 7 (2015) 16495–16506. doi:10.1021/acsami.5b03882.

[19] K. Devarayan, D. Lei, H.Y. Kim, B.S. Kim, Flexible transparent electrode based on PANi nanowire/nylon nanofiber reinforced cellulose acetate thin film as supercapacitor, Chem. Eng. J. 273 (2015) 603–609. doi:10.1016/j.cej.2015.03.115.

[20] C. (John) Zhang, T.M. Higgins, S.H. Park, S.E. O'Brien, D. Long, J.N. Coleman, V. Nicolosi, Highly flexible and transparent solid-state supercapacitors based on RuO_2/PEDOT:PSS conductive ultrathin films, Nano Energy. 28 (2016) 495–505. doi:10.1016/j.nanoen.2016.08.052.

[21] F. Chen, P. Wan, H. Xu, X. Sun, Flexible Transparent Supercapacitors Based on Hierarchical Nanocomposite Films, ACS Appl. Mater. Interfaces. 9 (2017) 17865–17871. doi:10.1021/acsami.7b02460.

[22] T. Cheng, Y.Z. Zhang, J.D. Zhang, W.Y. Lai, W. Huang, High-performance free-standing PEDOT:PSS electrodes for flexible and transparent all-solid-state supercapacitors, J. Mater. Chem. A. 4 (2016) 10493–10499. doi:10.1039/c6ta03537j.

[23] Y.H. Liu, J.L. Xu, S. Shen, X.L. Cai, L. Sen Chen, S.D. Wang, High-performance, ultra-flexible and transparent embedded metallic mesh electrodes by selective electrodeposition for all-solid-state supercapacitor applications, J. Mater. Chem. A. 5 (2017) 9032–9041. doi:10.1039/c7ta01947e.

[24] T. Cheng, Y.Z. Zhang, J.P. Yi, L. Yang, J.D. Zhang, W.Y. Lai, W. Huang, Inkjet-printed flexible, transparent and aesthetic energy storage devices based on PEDOT:PSS/Ag grid electrodes, J. Mater. Chem. A. 4 (2016) 13754–13763. doi:10.1039/c6ta05319j.

[25] J. Liu, G. Shen, S. Zhao, X. He, C. Zhang, T. Jiang, J. Jiang, B. Chen, A one-dimensional Ag NW@NiCo/NiCo(OH)$_2$ core-shell nanostructured electrode for a flexible and transparent asymmetric supercapacitor, J. Mater. Chem. A. 7 (2019) 8184–8193. doi:10.1039/c9ta01303b.

[26] J. Yu, J. Wu, H. Wang, A. Zhou, C. Huang, H. Bai, L. Li, Metallic Fabrics as the Current Collector for High-Performance Graphene-Based Flexible Solid-State Supercapacitor, (2016). doi:10.1021/acsami.5b12180.

[27] X. Liu, D. Li, X. Chen, W.Y. Lai, W. Huang, Highly Transparent and Flexible All-Solid-State Supercapacitors Based on Ultralong Silver Nanowire Conductive Networks, ACS Appl. Mater. Interfaces. 10 (2018) 32536–32542. doi:10.1021/acsami.8b10138.

[28] J.L. Xu, Y.H. Liu, X. Gao, Y. Sun, S. Shen, X. Cai, L. Chen, S.D. Wang, Embedded Ag Grid Electrodes as Current Collector for Ultraflexible Transparent Solid-State Supercapacitor, ACS Appl. Mater. Interfaces. 9 (2017) 27649–27656. doi:10.1021/acsami.7b06184.

[29] H. Moon, H. Lee, J. Kwon, Y.D. Suh, D.K. Kim, I. Ha, J. Yeo, S. Hong, S.H. Ko, Ag/Au/Polypyrrole Core-shell Nanowire Network for Transparent, Stretchable and Flexible Supercapacitor in Wearable Energy Devices, Sci. Rep. 7 (2017) 1–10. doi:10.1038/srep41981.

[30] S.B. Singh, T. Kshetri, T.I. Singh, N.H. Kim, J.H. Lee, Embedded PEDOT:PSS/AgNFs network flexible transparent electrode for solid-state supercapacitor, Chem. Eng. J. 359 (2019) 197–207. doi:10.1016/j.cej.2018.11.160.

[31] T. Qiu, B. Luo, M. Giersig, E.M. Akinoglu, L. Hao, X. Wang, L. Shi, M. Jin, L. Zhi, Au@MnO_2 core-shell nanomesh electrodes for transparent flexible supercapacitors, Small. 10 (2014) 4136–4141. doi:10.1002/smll.201401250.

[32] Y. Wang, W. Zhou, Q. Kang, J. Chen, Y. Li, X. Feng, D. Wang, Y. Ma, W. Huang, Patterning Islandlike MnO_2 Arrays by Breath-Figure Templates for Flexible Transparent Supercapacitors, ACS Appl. Mater. Interfaces. 10 (2018) 27001–27008. doi:10.1021/acsami.8b06710.

[33] H. Sheng, X. Zhang, Y. Ma, P. Wang, J. Zhou, Q. Su, W. Lan, E. Xie, C.J. Zhang, Ultrathin, Wrinkled, Vertically Aligned $Co(OH)_2$ Nanosheets/Ag Nanowires Hybrid Network for Flexible Transparent Supercapacitor with High Performance, ACS Appl. Mater. Interfaces. 11 (2019) 8992–9001. doi:10.1021/acsami.8b18609.

[34] G. Zhang, X.W.D. Lou, Controlled growth of $NiCo_2O_4$ nanorods and ultrathin nanosheets on carbon nanofibers for high-performance supercapacitors, Sci. Rep. 3 (2013) 2–7. doi:10.1038/srep01470.

[35] L. Huang, D. Chen, Y. Ding, S. Feng, Z.L. Wang, M. Liu, Nickel-cobalt hydroxide nanosheets coated on $NiCo_2O_4$ nanowires grown on carbon fiber paper for high-performance pseudocapacitors, Nano Lett. 13 (2013) 3135–3139. doi:10.1021/nl401086t.

[36] J. Xiao, X. Zeng, W. Chen, F. Xiao, S. Wang, High electrocatalytic activity of self-standing hollow $NiCo_2S_4$ single crystalline nanorod arrays towards sulfide redox shuttles in quantum dot-sensitized solar cells, Chem. Commun. 49 (2013) 11734–11736. doi:10.1039/c3cc44242j.

[37] Q. Liu, J. Jin, J. Zhang, $NiCo_2S_4$@graphene as a bifunctional electrocatalyst for oxygen reduction and evolution reactions, ACS Appl. Mater. Interfaces. 5 (2013) 5002–5008. doi:10.1021/am4007897.

[38] S. Peng, L. Li, C. Li, H. Tan, R. Cai, H. Yu, S. Mhaisalkar, M. Srinivasan, S. Ramakrishna, Q. Yan, In situ growth of $NiCo_2S_4$ nanosheets on graphene for high-performance supercapacitors, Chem. Commun. 49 (2013) 10178–10180. doi:10.1039/c3cc46034g.

[39] H. Chen, J. Jiang, L. Zhang, H. Wan, T. Qi, D. Xia, Highly conductive $NiCo_2S_4$ urchin-like nanostructures for high-rate pseudocapacitors, Nanoscale. 5 (2013) 8879–8883. doi:10.1039/c3nr02958a.

[40] L. Yu, L. Zhang, H. Bin Wu, X.W.D. Lou, Formation of $Ni_xCo_{3-x}S_4$ hollow nanoprisms with enhanced pseudocapacitive properties, Angew. Chemie - Int. Ed. 53 (2014) 3711–3714. doi:10.1002/anie.201400226.

[41] W. Chen, C. Xia, H.N. Alshareef, One-step electrodeposited nickel cobalt sulfide nanosheet arrays for high-performance asymmetric supercapacitors, ACS Nano. 8 (2014) 9531–9541. doi:10.1021/nn503814y.

[42] K.S. Anuratha, S. Mohan, S.K. Panda, Pulse reverse electrodeposited $NiCo_2S_4$ nanostructures as efficient counter electrodes for dye-sensitized solar cells, New J. Chem. 40 (2016) 1785–1791. doi:10.1039/c5nj02565f.

[43] S. K. Sami, S. Siddiqui, M. T. Feroze, and C-H. Chung, Electrodeposited nickel-cobalt sulfide nanosheet on polyacrylonitrile nanofibers: A Binder-free electrode for flexible supercapacitors, Mater. Res. Express 4 (2017), 116309.

[44] A. Irshad, N. Munichandraiah, Electrodeposited Nickel-Cobalt-Sulfide Catalyst for the Hydrogen Evolution Reaction, ACS Appl. Mater. Interfaces. 9 (2017) 19746–19755. doi:10.1021/acsami.6b15399.

[45] J. Yin, Y. Wang, W. Meng, T. Zhou, B. Li, T. Wei, Y. Suna, Honeycomb-like $NiCo_2S_4$ nanosheets prepared by a rapid electrodeposition as a counter electrode for dye-sensitized solar cells, Nanotechnology, 28 (2017) 345403.

[46] H. Wu, D. Kong, Z. Ruan, P.C. Hsu, S. Wang, Z. Yu, T.J. Carney, L. Hu, S. Fan, Y. Cui, A transparent electrode based on a metal nanotrough network, Nat. Nanotechnol. 8 (2013) 421–425. doi:10.1038/nnano.2013.84.

[47] J. Chen, J. Chen, Y. Li, W. Zhou, X. Feng, Q. Huang, J.G. Zheng, R. Liu, Y. Ma, W. Huang, Enhanced oxidation-resistant Cu-Ni core-shell nanowires: Controllable one-pot synthesis and solution processing to transparent flexible heaters, Nanoscale. 7 (2015) 16874–16879. doi:10.1039/c5nr04930j.

[48] A.R. Rathmell, M. Nguyen, M. Chi, B.J. Wiley, Synthesis of oxidation-resistant cupronickel nanowires for transparent conducting nanowire networks, Nano Lett. 12 (2012) 3193–3199. doi:10.1021/nl301168r.

[49] K. Kim, H.C. Kwon, S. Ma, E. Lee, S.C. Yun, G. Jang, H. Yang, J. Moon, All-Solution-Processed Thermally and Chemically Stable Copper-Nickel Core-Shell Nanowire-Based Composite Window Electrodes for Perovskite Solar Cells, ACS Appl. Mater. Interfaces. 10 (2018) 30337–30347. doi:10.1021/acsami.8b09266.

[50] P.C. Hsu, H. Wu, T.J. Carney, M.T. McDowell, Y. Yang, E.C. Garnett, M. Li, L. Hu, Y. Cui, Passivation coating on electrospun copper nanofibers for stable transparent electrodes, ACS Nano. 6 (2012) 5150–5156. doi:10.1021/nn300844g.

[51] S.B. Singh, Y. Hu, T. Kshetri, N.H. Kim, J.H. Lee, An embedded-PVA@Ag nanofiber network for ultra-smooth, high performance transparent conducting electrodes, J. Mater. Chem. C. 5 (2017) 4198–4205. doi:10.1039/c7tc01002h.

[52] G. Nagaraju, S. Chandra Sekhar, L. Krishna Bharat, J.S. Yu, Wearable Fabrics with Self-Branched Bimetallic Layered Double Hydroxide Coaxial Nanostructures for Hybrid Supercapacitors, ACS Nano. 11 (2017) 10860–10874. doi:10.1021/acsnano.7b04368.

[53] H.C. Chen, Y. Qin, H. Cao, X. Song, C. Huang, H. Feng, X.S. Zhao, Synthesis of amorphous nickel–cobalt–manganese hydroxides for supercapacitor-battery hybrid energy storage system, Energy Storage Mater. 17 (2019) 194–203. doi:10.1016/j.ensm.2018.07.018.

[54] W. Zhou, X. Cao, Z. Zeng, W. Shi, Y. Zhu, Q. Yan, H. Liu, J. Wang, H. Zhang, One-step synthesis of Ni_3S_2 nanorod@$Ni(OH)_2$ nanosheet core-shell nanostructures on a three-dimensional graphene network for high-performance supercapacitors, Energy Environ. Sci. 6 (2013) 2216–2221. doi:10.1039/c3ee40155c.

[55] X. Xia, C. Zhu, J. Luo, Z. Zeng, C. Guan, C.F. Ng, H. Zhang, H.J. Fan, Synthesis of free-standing metal sulfide nanoarrays via anion exchange reaction and their electrochemical energy storage application, Small. 10 (2014) 766–773. doi:10.1002/smll.201302224.

[56] W. Du, Z. Wang, Z. Zhu, S. Hu, X. Zhu, Y. Shi, H. Pang, X. Qian, Facile synthesis and superior electrochemical performances of $CoNi_2S_4$/graphene nanocomposite suitable for

supercapacitor electrodes, J. Mater. Chem. A. 2 (2014) 9613–9619. doi:10.1039/c4ta00414k.

[57] W. Chen, R.B. Rakhi, L. Hu, X. Xie, Y. Cui, H.N. Alshareef, High-performance nanostructured supercapacitors on a sponge, Nano Lett. 11 (2011) 5165–5172. doi:10.1021/nl2023433.

[58] J. Pu, T. Wang, H. Wang, Y. Tong, C. Lu, W. Kong, Z. Wang, Direct growth of $NiCo_2S_4$ nanotube arrays on nickel foam as high-performance binder-free electrodes for supercapacitors, Chempluschem. 79 (2014) 577–583. doi:10.1002/cplu.201300431.

[59] T. Wang, B. Zhao, H. Jiang, H.P. Yang, K. Zhang, M.M.F. Yuen, X.Z. Fu, R. Sun, C.P. Wong, Electro-deposition of $CoNi_2S_4$ flower-like nanosheets on 3D hierarchically porous nickel skeletons with high electrochemical capacitive performance, J. Mater. Chem. A. 3 (2015) 23035–23041. doi:10.1039/c5ta04705f.

[60] J. Yang, C. Yu, X. Fan, S. Liang, S. Li, H. Huang, Z. Ling, C. Hao, J. Qiu, Electroactive edge site-enriched nickel-cobalt sulfide into graphene frameworks for high-performance asymmetric supercapacitors, Energy Environ. Sci. 9 (2016) 1299–1307. doi:10.1039/c5ee03633j.

[61] W. Hu, R. Chen, W. Xie, L. Zou, N. Qin, D. Bao, $CoNi_2S_4$ nanosheet arrays supported on nickel foams with ultrahigh capacitance for aqueous asymmetric supercapacitor applications, ACS Appl. Mater. Interfaces. 6 (2014) 19318–19326. doi:10.1021/am5053784.

[62] K.M. Abraham, S.M. Chaudhri, The Lithium Surface Film in the Li/SO_2 Cell, J. Electrochem. Soc. 133 (1986) 1307–1311. doi:10.1149/1.2108858.

[63] A.B. Christie, J. Lee, I. Sutherland, J.M. Walls, An XPS study of ion-induced compositional changes with group II and group IV compounds, Appl. Surf. Sci. 15 (1983) 224–237. doi:10.1016/0378-5963(83)90018-1.

[64] X. Han, Y. Yang, J.J. Zhou, Q. Ma, K. Tao, L. Han, Metal–Organic Framework Templated 3D Hierarchical $ZnCo_2O_4$@$Ni(OH)_2$ Core–Shell Nanosheet Arrays for High-Performance Supercapacitors, Chem. - A Eur. J. 24 (2018) 18106–18114. doi:10.1002/chem.201804327.

[65] Z. Li, X. Yu, A. Gu, H. Tang, L. Wang, Z. Lou, Anion exchange strategy to synthesis of porous NiS hexagonal nanoplates for supercapacitors, Nanotechnology. 28 (2017). doi:10.1088/1361-6528/28/6/065406.

[66] J. Shi, X. Li, G. He, L. Zhang, M. Li, Electrodeposition of high-capacitance 3D CoS/graphene nanosheets on nickel foam for high-performance aqueous asymmetric supercapacitors, J. Mater. Chem. A. 3 (2015) 20619–20626. doi:10.1039/c5ta04464b.

[67] S. Shahrokhian, L. Naderi, High-Performance, Flexible, All-Solid-State Wire-Shaped Asymmetric Micro-Supercapacitors Based on Three Dimensional $CoNi_2S_4$ Nanosheets Decorated-Nanoporous Ni-Zn-P Film/Cu Wire, J. Phys. Chem. C. 123 (2019) 21353–21366. doi:10.1021/acs.jpcc.9b04718.

[68] R.T. Ginting, M.M. Ovhal, J.W. Kang, A novel design of hybrid transparent electrodes for high performance and ultra-flexible bifunctional electrochromic-supercapacitors, Nano Energy. 53 (2018) 650–657. doi:10.1016/j.nanoen.2018.09.016.

[69] C.J. Zhang, B. Anasori, A. Seral-Ascaso, S.H. Park, N. McEvoy, A. Shmeliov, G.S. Duesberg, J.N. Coleman, Y. Gogotsi, V. Nicolosi, Transparent, Flexible, and Conductive

2D Titanium Carbide (MXene) Films with High Volumetric Capacitance, Adv. Mater. 29 (2017) 1–9. doi:10.1002/adma.201702678.

[70] K. Lee, H. Lee, Y. Shin, Y. Yoon, D. Kim, H. Lee, Highly transparent and flexible supercapacitors using graphene-graphene quantum dots chelate, Nano Energy. 26 (2016) 746–754. doi:10.1016/j.nanoen.2016.06.030.

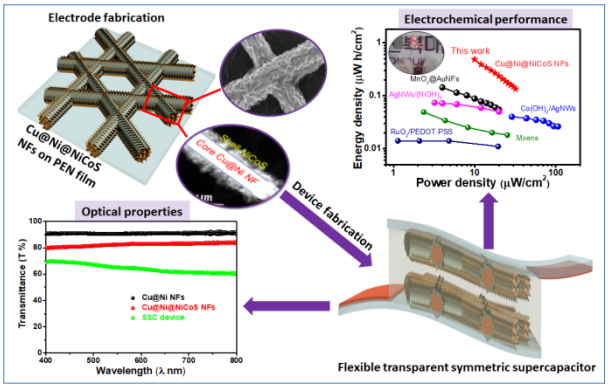

Highlights

- Cu@Ni@NiCoS core-shell nanofiber network electrode structured was fabricated.
- Cu@Ni NFs network electrode exhibit excellent chemical stability.
- Cu@Ni@NiCoS NFs network electrode shows excellent electro-optical performance.
- The electrode exhibits a high areal capacity of 6.94 μA h/cm^2 at ~76% transmittance.
- The device demonstrates a high energy density of ~0.48 μWh/cm^2 at ~11.15 μW/cm^2 power density.